Climate Dynamics (2001) 17: 735–751

A. Ganopolski · V. Petoukhov · S. Rahmstorf
V. Brovkin · M. Claussen · A. Eliseev · C. Kubatzki

CLIMBER-2: a climate system model of intermediate complexity. Part II: model sensitivity

Received: 28 May 2000 / Accepted: 9 November 2000

Abstract A set of sensitivity experiments with the climate system model of intermediate complexity CLIMBER-2 was performed to compare its sensitivity to changes in different types of forcings and boundary conditions with the results of comprehensive models (GCMs). We investigated the climate system response to changes in freshwater flux into the Northern Atlantic, CO_2 concentration, solar insolation, and vegetation cover in the boreal zone and in the tropics. All these experiments were compared with the results of corresponding experiments performed with different GCMs. Qualitative, and in many respects, quantitative agreement between the results of CLIMBER-2 and GCMs demonstrate the ability of our climate system model of intermediate complexity to address diverse aspects of the climate change problem. In addition, we used our model for a series of experiments to assess the impact of some climate feedbacks and uncertainties in model parameters on the model sensitivity to different forcings. We studied the role of freshwater feedback and vertical ocean diffusivity for the stability properties of the thermohaline ocean circulation. We show that freshwater feedback plays a minor role, while changes of vertical diffusivity in the ocean considerably affect the circulation stability. In global warming experiments we analysed the impact of hydrological sensitivity and vertical diffusivity on the long-term evolution of the thermohaline circulation. In the boreal and tropical deforestation experiments we assessed the role of an interactive ocean and showed that for both types of deforestation scenarios, an interactive ocean leads to an additional cooling due to albedo and water vapour feedbacks.

A. Ganopolski (✉) · V. Petoukhov · S. Rahmstorf
V. Brovkin · M. Claussen · C. Kubatzki
Potsdam Institute for Climate Impact Research,
P.O. Box 601203, 14412 Potsdam, Germany
E-mail: andrey@pik-potsdam.de

A. Eliseev
A.M. Obukhov Institute for Atmospheric Physics,
Pyzhevsky 3, 109017 Moscow, Russia

Also at:
M. Claussen, Institut für Meteorologie,
Freie Universität Berlin, Carl-Heinrich Weg 6-10,
12165 Berlin, Germany

1 Introduction

In the first part of the study (Petoukhov et al. 2000) we described the climate system model of intermediate complexity CLIMBER-2 and its performance for the present-day climate. We have shown that the model is able to simulate present-day climate fairly realistically. The purpose of this second part is to compare the results of sensitivity experiments performed with our model and GCMs. This comparison, together with the simulations of the present and past climates, is an important part of the assessment of the quality and the range of applicability of the CLIMBER-2 model.

Experiments were chosen with respect to the importance of forcings and changes in boundary conditions for the potential applications of our model, as well as for the availability of similar experiments performed with comprehensive climate models. We present the model sensitivity to changes in:

1. Freshwater flux into the Northern Atlantic
2. Atmospheric CO_2 concentration
3. Temporal variability of solar insolation
4. Vegetation cover in the boreal zone and in the tropics

When comparing the results of our model and GCMs, the obvious problem is that different models yield different results. We present the results of our sensitivity experiments irrespective of whether or not corresponding results of GCMs are unambiguous. It is important to stress that CLIMBER-2 is not designed to mimic any specific GCM, it is a climate model in its own right, although a simplified one. CLIMBER-2 was used

already for simulations of the Last Glacial Maximum (Ganopolski et al. 1998a) and mid-Holocene (Ganopolski et al. 1998b) climates, a transient Holocene simulation (Claussen et al. 1999), historical climatic changes during the last millennia (Brovkin et al. 1999) and future climatic change scenarios (Rahmstorf and Ganopolski 1999). In those experiments the changes in the forcings and boundary conditions considered here were involved in different combinations. A detailed study of the model sensitivity to each of these changes separately helps to understand the combined effect of several factors.

Some similar sensitivity experiments have been previously performed with another climate models of intermediate complexity. Stocker and Wright (1991) analysed the response of the thermohaline circulation to the changes in freshwater flux. Stocker and Schmittner (1997) and Sokolov and Stone (1998) performed a series of experiments for different CO_2 scenarios, and Bertrand et al. (1999) studied the climate response to changes in solar insolation. However, the entire set of experiments described here has not yet been performed either with the same GCM or with simplified models. This is why we believe that the fact that many important results obtained with GCMs can be reproduced with one, relatively simple and coarse resolution model is encouraging and gives additional credibility to these results. Due to the low computational cost of our model we performed additional sensitivity experiments to facilitate an understanding of the possible reasons for discrepancies between the results of different climate models. This type of study is a natural application for a model of intermediate complexity, designed as a complimentary tool (to GCMs) for climate studies.

2 Sensitivity of the thermohaline ocean circulation to freshwater flux

The problem of stability and variability of the oceanic thermohaline circulation has recently attracted much attention due to its importance for past and future climate changes (e.g. Manabe and Stouffer 1994; Rahmstorf 1999). This problem was addressed in numerous studies using a range of the models, from simple box models up to coupled AOGCMs. Bryan (1986) first showed the existence of multiple equilibria of the thermohaline circulation in an OGCM driven by mixed boundary conditions at the surface. Two radically different equilibria of the climate system for the present-day external conditions were found by Manabe and Stouffer (1988) using the GFDL coupled climate model. They speculated that the climate state corresponding to the conveyor-off mode could be considered as an analog of cold Younger-Dryas event (around 12 500 before present). Schiller et al. (1997), using the ECHAM3/LSG coupled GCM, found two similar states with conveyor-on and -off modes of the thermohaline circulation, but the conveyor-off mode existed only when a large anomalous freshwater flux was applied to the Northern Atlantic. After this anomalous freshwater flux ceased, the thermohaline circulation returned to the conveyor-on regime within a few hundred years. Two different modes of thermohaline circulation were also obtained using a hybrid climate model (ocean GCM coupled to an energy balance atmosphere), Fanning and Weaver (1997). Rahmstorf (1996) (hereafter R96) performed systematic studies of the sensitivity of the thermohaline circulation to changes in freshwater flux into the Atlantic basin. He showed that there is a range of freshwater forcing where two different equilibria (conveyor-on and conveyor-off) exist and that the sensitivity of the thermohaline circulation to changes in freshwater flux and the number of possible equilibria depend on the total Atlantic freshwater balance. Qualitatively similar results were obtained with the zonally averaged ocean model by Stocker and Wright (1991).

2.1 Thermohaline circulation hysteresis

Using CLIMBER-2 we performed experiments similar to R96, tracing the quasi-equilibrium dependence of the Atlantic thermohaline circulation on freshwater flux. In this experiment (refered hereafter as HYS, see complete list of experiment acronyms in Table 1) we add an additional freshwater flux in the latitude belt 40–60°N in the North Atlantic, with compensation of the freshwater flux perturbation over the Pacific and Indian oceans to keep the globally averaged salinity constant. We use the same rate

Table 1 List of the acronyms of different experiments used

Equilibrium experiments	
CE	Equilibrium climate state corresponding to conveyor-on mode of the thermohaline circulation (described in detail in Petoukhov et al. 2000)
CE_OFF	Equilibrium climate state corresponding to conveyor-off mode
CE_LVD	Equilibrium climate state with large vertical diffusivity (1.5 cm^2/s)
CE_SVD	Equilibrium climate state with small vertical diffusivity (0.3–1.3 cm^2/s)
C2	Equilibrium doubling CO_2 experiment
Freshwater hysteresis experiments	
HYS	Hysteresis experiment with standard set of parameters
HYS_FWC	Hysteresis experiment with freshwater feedback switched off
HYS_LVD	Hysteresis experiment with large vertical diffusivity
Transient CO_2 experiments	
CT2	Transient doubling CO_2 experiment
CT4	Transient quadrupling CO_2 experiment
CT4_EHS	As CT4 but with enhanced hydrological sensitivity
CT4_SVD	As CT4 but with smaller vertical diffusivity
CT4_EHS_SVD	As CT4 but with combination of enhanced hydrological sensitivity and small vertical diffusivity
Boreal deforestation	
BD_A	Boreal forest is replaced by desert, atmosphere only model
BD_AO	Boreal forest is replaced by desert, coupled model
BG_A	Boreal forest is replaced by grassland, atmosphere only model
BG_AO	Boreal forest is replaced by grassland, coupled model
Tropical deforestation	
TD_A	Tropical forest is replaced by desert, atmosphere only model
TD_AO	Tropical forest is replaced by desert, coupled model
TG_A	Tropical forest is replaced by grassland, atmosphere only model
TG_AV	Tropical forest is replaced by grassland, coupled model

(0.05 Sv/kyr) of changes in freshwater flux as R96, slow enough to allow the ocean to be in quasi-equilibrium with the external forcing. Tracing the entire loop of the thermohaline hysteresis takes about 25 000 model years. Our model is rather different from the one used in R96 in formulation and resolution, but both models are similar in respect to the intensity of the oceanic overturning (Fig. 1a) and meridional freshwater flux in the Atlantic two key factors determining the stability of the thermohaline circulation.

The response of the maximum overturning in the Northern Atlantic to the perturbation in the freshwater flux is depicted in Fig. 2a. The shape of the hysteresis curve and the range of freshwater fluxes where two equilibria exist (0.2 Sv) simulated with our model are very similar to R96 although the whole diagram is shifted towards the higher values of the freshwater fluxes by 0.1 Sv or, in other words, the present-day climate equilibrium is located farther to the left on the hysteresis loop. The thermohaline circulation collapsed in our model when the additional freshwater flux exceeds 0.2 Sv. At the same time, the conveyor-on mode recovers only when a negative freshwater anomaly is applied. This implies that the model has two stable equilibria for present-day conditions (states A and B in Fig. 2a), similar to R96 and Manabe and Stouffer (1988).

One important difference between our experiment and R96 is that in the latter the perturbation of freshwater flux was added to a fixed freshwater flux diagnosed in the control simulation, while in our experiments the anomalous freshwater flux was added to the flux calculated by the coupled model. Since changes in thermohaline circulation affect the sea surface temperature and the hydrological cycle, the simulated freshwater flux is affected by the applied perturbation. Nakamura et al. (1994) and Scott et al. (1999), using 2 and 3-box models of the thermohaline circulation coupled to a simple atmospheric model, argued that this feedback between thermohaline circulation and meridional moisture transport in the atmosphere is positive and may play an important role in destabilising the thermohaline circulation. To estimate the role of this feedback in our model, we performed an additional experiment (referred as HYS_FWC), where the perturbation of freshwater flux was added to a fixed freshwater flux diagnosed from the equilibrium present-day climate state (experiments referred hereafter as CE). In respect of changes in the freshwater flux experiment HYS_FWC is identical to R96, and the feedback between thermohaline circulation and freshwater flux is excluded. As seen from Fig. 2a, this feedback indeed decreases the stability of the thermohaline circulation, but the difference in critical perturbation of freshwater flux which leads to a shutdown of the thermohaline circulation is very small (0.02 Sv). Thus our results support the conclusion of Hughes and Weaver (1996), that positive feedback

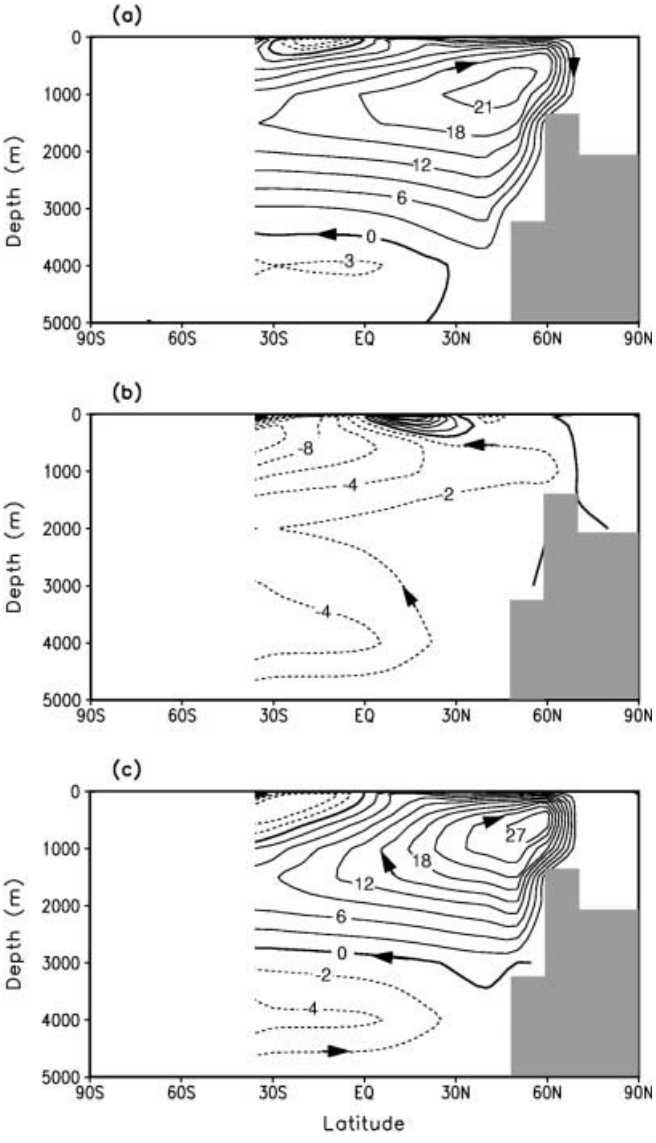

Fig. 1a–c Meridional overturning stream function in Sv in the Atlantic for **a** CE experiment, **b** CE_OFF experiment, and **c** CE_LVD experiment

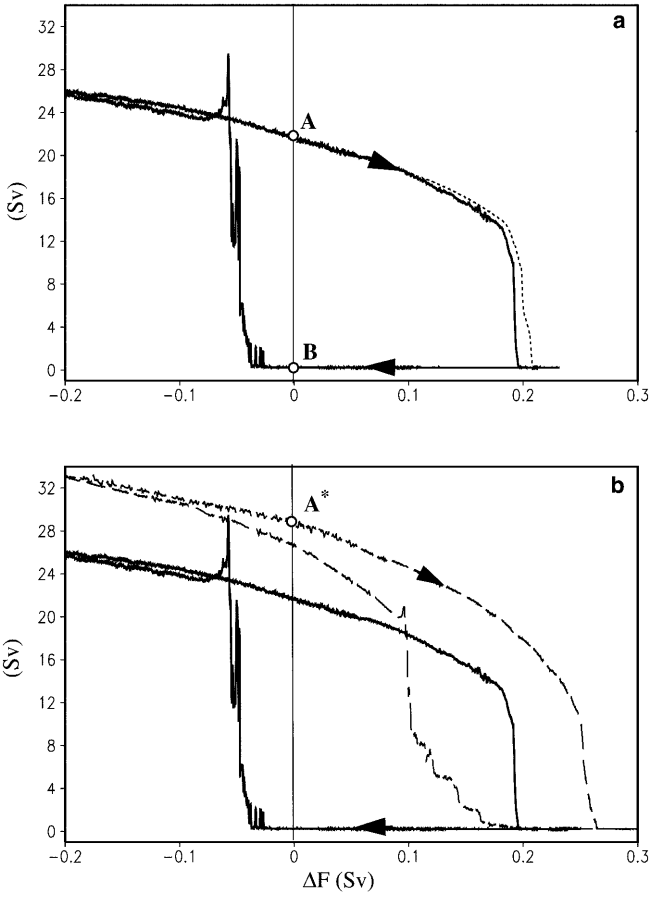

Fig. 2a, b Hysteresis response of the North Atlantic overturning to a slowly changing freshwater forcing. **a** HYS experiment (*solid line*) and HYS_FWC (*dashed line*). **b** HYS experiment (*solid line*) and HYS_LVD experiment (*dashed line*)

between the thermohaline circulation and freshwater flux does not play an important role.

Recently, Manabe and Stouffer (1999) proposed an explanation for the fact that the GFDL model has two stable equilibria for present-day climate, while the ECHAM/LSG model shows only one (conveyor-on) stable equilibrium (Schiller et al. 1997). By increasing the vertical diffusivity in the ocean model, to mimic the large numerical diffusivity in the LSG model, Manabe and Stouffer (1999) were able to change the stability properties of their model so that it possesses only one (conveyor-on) stable equilibrium of thermohaline circulation. To test if our model shows similar behaviour we made an experiment with increased vertical diffusivity. Vertical profiles of vertical diffusion coefficients in the CLIMBER-2 and GFDL models have the same shape with smaller diffusivity in the upper two kilometres of the ocean and higher diffusivity in the deep ocean. The only difference is that in the GFDL model vertical diffusivity varies between 0.3 and 1.3 cm^2/s, while in our model the range is 0.5 to 1.5 cm^2/s. For comparison with Manabe and Stouffer (1999), we performed an additional experiment with constant vertical diffusivity of 1.5 cm^2/s (Manabe and Stoffer (1999) used constant vertical diffusivity of 1.3 cm^2/s). First we simulated new equilibrium climate state corresponding this vertical diffusivity (experiments CE_LVD). Similar to Manabe and Stouffer (1999) (Fig. 1c), the maximum of the North Atlantic overturning increases from 21 Sv in experiment CE to 29 Sv in experiment CE_LVD, while the outflow out of the Atlantic at 30°S was hardly affected. Climate characteristics and freshwater flux to the Atlantic ocean do not change much compared to CE. Then we performed a hysteresis experiment with large vertical diffusivity (experiment HYS_LVD) using the same procedure as in experiment HYS. Figure 2b shows that the hysteresis behaviour in experiment HYS_LVD differs substantially from HYS. The thermohaline circulation becomes more stable, which implies that a larger perturbation of freshwater flux has to be applied to shut down the conveyor. The range of freshwater flux where the model has two equilibria is substantially reduced and the position of the recovery point now migrates to the area of positive freshwater fluxes. This means that in HYS_LVD for unperturbed conditions there is only one equilibrium A* corresponding to the conveyor-on mode. Thus our model shows the same sensitivity of the stability of the thermohaline circulation to an increase of vertical diffusivity as the GFDL model and our results confirm that the stability properties of the thermohaline circulation are sensitive to vertical diffusivity.

2.2 Two climate equilibria

The points A and B in Fig. 2a correspond to conveyor-on and conveyor-off modes of the thermohaline circulation. Since the HYS experiment is transient (although with a very small rate of change) both climate states are not strictly equilibria of the climate system. The climate state corresponding to point A is close to the equilibrium CE described in Petoukhov et al. (2000). To compute the second equilibrium climate state, we performed an additional experiment with constant external forcings, using state B as initial condition. After 5000 years of integration a new equilibrium corresponding to the conveyor-off mode of the thermohaline circulation (referred hereafter as CE_OFF) was obtained. These two equilibria CE and CE_OFF are stable with respect to small perturbations of the freshwater flux and correspond to the two climate states obtained by Manabe and Stouffer (1988). We will also compare our results with Schiller et al. (1997). Because the latter is not an equilibrium but transient response of the climate system to a collapse of the thermohaline circulation, some differences, especially in the Southern Hemisphere, can be expected.

Figure 1a, b shows the patterns of the vertical overturning in the Atlantic for CE and CE_OFF experiments. In CE_OFF the formation of NADW has ceased completely and a reverse cell of meridional circulation occupies the whole Atlantic ocean. Maximum northward meridional heat transport in the Northern Atlantic in CE_OFF is only 0.1 PW compared to 1 PW in CE. As a result, SST in the Northern Atlantic in CE_OFF is up to 7 K lower than in CE and salinity is lower by 3–5 ppt. These features of changes in oceanic state due to the collapse of the thermohaline circulation agree with the results of coupled GCMs (Manabe and Stouffer 1988; Schiller et al. 1997) and R96.

Figure 3 shows winter and annual differences in air temperature, and annual differences in precipitation and sea level pressure between the conveyor-off and -on modes. The model predicts a maximum cooling over the Northern Atlantic (60°N–70°N) annually by 7 K and in winter up to 15 K. This cooling is caused by a reduction of the Northward oceanic heat transport and amplified by a 30% increase in sea-ice area in the Northern Atlantic. The area of pronounced cooling occupies the high and middle latitudes over the whole Northern Hemisphere. Due to the reduction of the northward heat transport in the Atlantic, the Southern Hemisphere temperature increases with the maximum warming in the high latitudes of the Southern Atlantic. These results agree favourably with Manabe and Stouffer (1988) and Schiller et al. (1997), although the ECHAM/LSG model produces a stronger cooling over the Northern Atlantic and a weaker warming in the Southern Hemisphere compared to our results and to Manabe and Stouffer (1988).

In CE_OFF precipitation decreases compared to CE over a large portion of the Northern Hemisphere, with the largest negative anomalies over the Northern Atlantic, where annual precipitation decreases by 1 mm/day. At the same time, precipitation increase slightly over North America and the North Pacific, due to the changes in atmospheric circulation. In the tropics negative precipitation anomalies are located northward of the equator and positive anomalies southward of the equator. These changes can be attributed to changes in the atmospheric meridional circulation, namely an intensification of the northern and a weakening of the southern Hadley cell, and a southward shift of the ITCZ, as reported in Ganopolski et al. (1998a) (their Fig. 5b). These changes in the meridional circulation are caused by the cooling of the Northern Hemisphere and warming of the Southern Hemisphere and are present in both GCM simulations. Like other characteristics, the largest changes in sea level pressure (Fig. 3d) occur over the Northern Atlantic and are strongest in winter (not shown). The pressure anomalies create an anomalous anticyclonic atmospheric circulation over the Atlantic and Europe, while over the Eastern North Pacific and North America a cyclonic anomaly in the atmospheric circulation is developed. In the Southern Hemisphere sea level pressure decreases in the subtropics and increases in the high latitudes. These patterns agree with GCM simulations.

3 Sensitivity to the changes in CO_2 concentration

Due to its practical importance, the largest number of GCM experiments was dedicated to the study of climate sensitivity to changes in atmospheric CO_2 concentration. In the 1980s most of these experiments were performed using atmospheric GCMs with simple mixed-layer ocean, allowing to study only an equilibrium response to changes in CO_2 concentration (e.g. Washington and Meehl 1984; Schlesinger and Mitchell 1987; Manabe and Wetherald 1987). In the 1990s a growing number of coupled atmosphere-ocean GCMs were used for transient (usually century scale) simulations for different CO_2 scenarios (Manabe et al. 1991; Cubasch et al. 1992; Cai and Gordon 1998; Wood et al. 1999). Some experiments also include other greenhouse gases and aerosols. In many of these experiments models with artificial flux adjustment at the air-sea interface were used. The role of flux adjustment and the climate drift problem are still

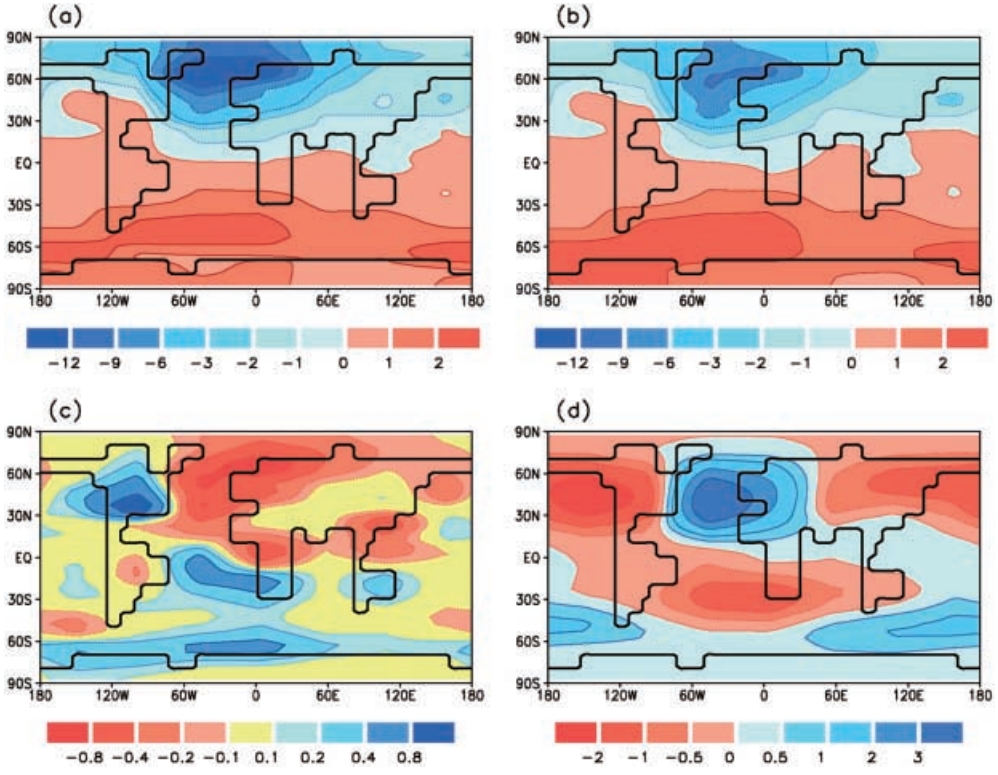

Fig. 3a–d Differences between CE_OFF and CE experiments. **a** Winter air temperature, **b** annual air temperature, **c** annual precipitation in mm/day, **d** sea level pressure in HPa

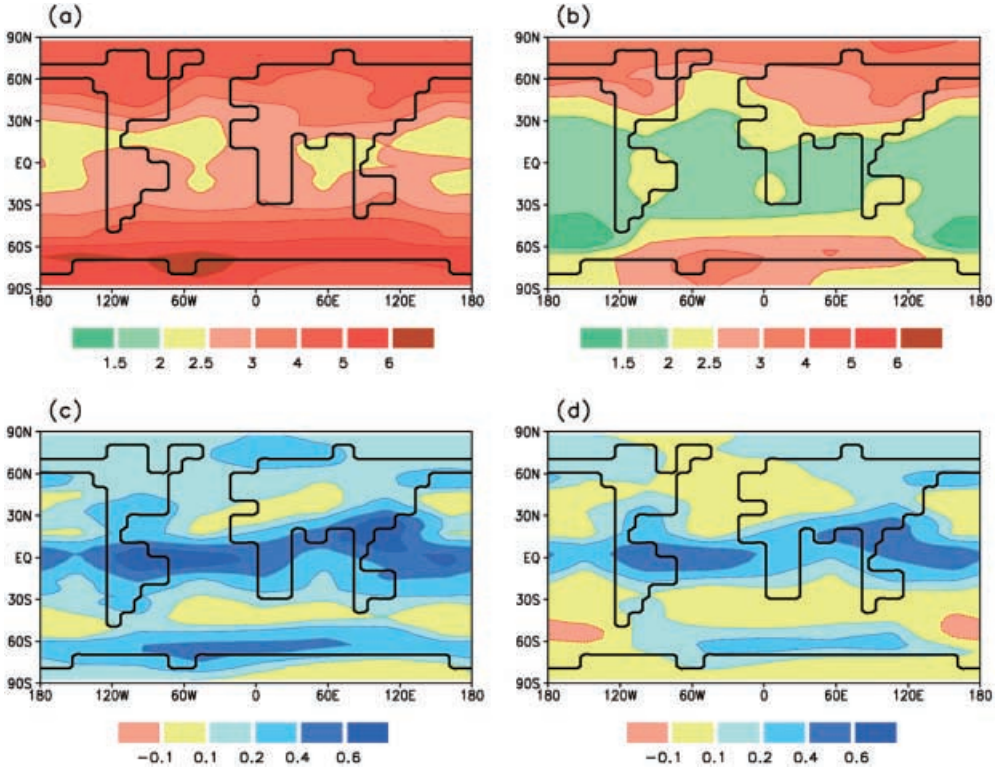

Fig. 4a, c Equilibrium and **b, d** transient annual climatic changes due to a doubling of CO_2 concentration. **a, b** Surface air temperature changes, **c, d** precipitation changes in (mm/day)

debated (see e.g. Houghton et al. 1996). In spite of the large number of experiments performed, there are still considerable uncertainties in climate response to changes in CO_2. For example, the global temperature sensitivity to a doubling of CO_2 (the climate sensitivity) ranges from 1.5 to 4.5 K in different GCMs (Houghton et al. 1996). Larger uncertainties also apply to changes in hydrological cycle, cloudiness, ocean circulation, etc.

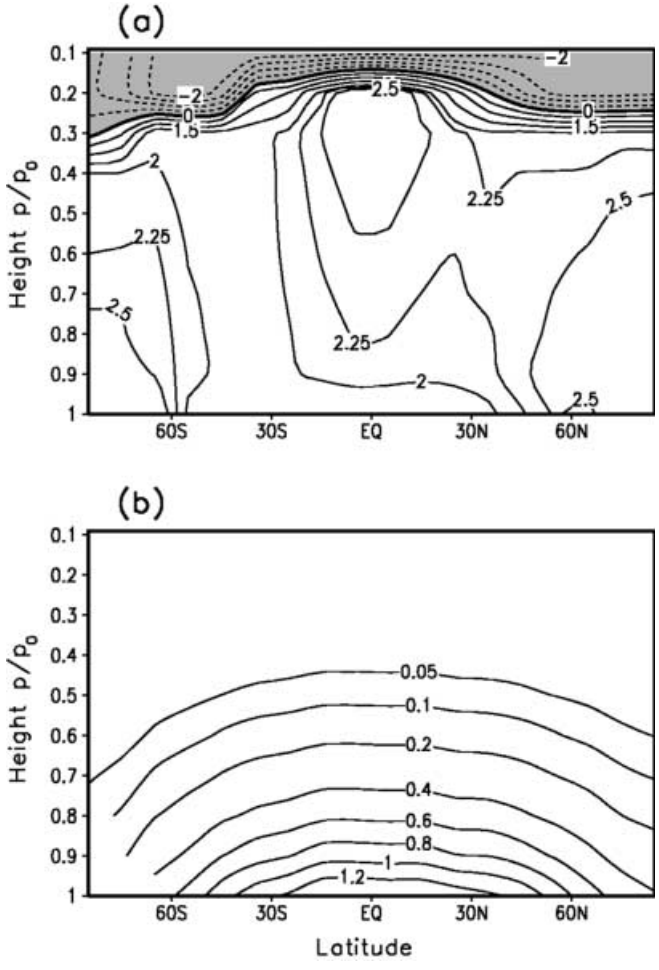

Fig. 5 Zonally and annually averaged changes in **a** atmosphere temperature and **b** specific humidity in g/kg for the equilibrium $2 \times CO_2$ experiment

Nevertheless a study of the model sensitivity to changes in CO_2 concentration provides the best opportunity to compare our model with the majority of GCMs.

3.1 Equilibrium $2 \times CO_2$ climate

First we will describe the equilibrium climate response to a doubling of CO_2 concentration. The model was run for 5000 years with doubled CO_2 concentration using the results of the CE experiment as initial condition. Table 2 summarises the changes in globally averaged climate characteristics for a CO_2 doubling experiment. The model climate sensitivity of 2.6 K is in the middle of the range of GCM experiments. It is important to recall that CLIMBER-2 climate sensitivity is not prescribed (as in energy balance models) but is a result of radiative forcing of CO_2 calculated with a multi-level radiation scheme (Petoukhov et al. 2000) and interaction between different feedbacks (water vapour, snow-ice-albedo, cloudiness, etc.) which are explicitly described in the model. Geographical patterns of the

Table 2 Differences in the globally averaged climate characteristics between doubled CO_2 and present-day climates in equilibrium and transient experiments. Numbers in brackets show relative (to the absolute values at present-day) changes

	Equilibrium	Transient
Δ surface air temperature, K	2.63	1.67
Δ planetary albedo, %	−0.8	−0.3
Δ surface albedo, %	−1.2	−0.7
Δ top energy balance, W/m^2	0.0	1.6
Δ downward LWR, W/m^2	14.5	9.5
Δ net surface radiation, W/m^2	3.1	2.8
Δ surface latent heat flux, W/m^2	7.5	4.8
Δ sensible heat, W/m^2	−4.3	−3.5
Δ precipitable water, mm	3.3	2.1
Δ precipitation, mm/d	0.23 (8%)	0.14 (5%)
Δ run-off, 10^{15} kg/yr	4.7 (13%)	3.1 (9%)
Δ cloudiness, %	−1.3	−1.2
Δ SST, K	1.8	0.9

annual temperature and precipitation changes are shown in Fig. 4 in comparison with the results of a transient experiment which will be discussed later. The poleward amplification of the warming which is seen in the figure is typical for all global warming simulations with different types of climate models. In the Southern Hemisphere the maximum temperature increase (above 5 K) is observed near Antarctica. Warming over the continents is typically higher by 0.5 K than over the oceans at the same latitudes. The vertical structure of the zonally averaged annual temperature changes in the atmosphere (Fig. 5a) resembles GCM results in the most important features. In the tropics, due to an increase of specific humidity and cumulus cloudiness, the lapse rates decreases and maximum warming occurs in the upper troposphere. In the high latitudes, in contrast, the lapse rate increases and maximum warming is near the surface. In the stratosphere temperature drops by up to 2 K, very close to the result of GCM simulations. Changes in specific humidity (Fig. 5b) are primarily the result of an increase in surface temperature and the assumed exponential vertical profile of specific humidity with a constant vertical length scale. The results of simulations with GCMs, (e.g. the GENESIS climate model, Thompson and Pollard 1995) confirm that in first approximation the changes in specific humidity due to an increase in CO_2 concentration have the same universal vertical structure as the specific humidity for the present-day climate. Thus, in spite of the fact that the vertical structure of temperature and humidity in our model is only diagnosed using surface characteristics and simple linear/exponential dependencies from height, the simulated changes of 3-D temperature/humidity agree with GCM results. As a result, simulated changes in radiative fluxes are also consistent with GCMs.

Global precipitation increases by 8%, which is on the "wet" side of the relation between climate sensitivity and global precipitation changes for different GCM experiments (Houghton et al. 1990). The largest increase in

precipitation occurs in the tropical zone (Fig. 4c). A secondary maximum of precipitation increase is located over the Southern Ocean, where the relative increase of precipitation exceeds 30%. An increase of precipitation in the middle and high latitudes of the Northern Hemisphere is much less pronounced. In this respect our results differ from the GFDL and some other GCMs which show the strongest increase of precipitation in the boreal zone of the Northern Hemisphere. This difference in precipitation changes explains the differences in the Atlantic hydrological sensitivity which will be discussed later. At the same time, even zonally averaged annual changes in precipitation vary significantly from one model to another. CLIMBER-2 simulates in summer (not shown) a strong intensification of the eastern Asian monsoon and a decrease of precipitation over Southern Europe. These changes are reported in many GCM simulations (see e.g. Kittel et al. 1998). At the same time a strong increase of precipitation, simulated in our model over equatorial Southern America, is far less robust. Some models, like HadCM3 (Mitchell et al. 1998), show a strong decline of precipitation in this region.

Seasonal variations of the zonally averaged climate changes are shown in Fig. 6. One can see a strong seasonal variation of the temperature anomalies in the high latitudes in both hemispheres, with the maximum warming in winter and minimum in summer, typical of global warming simulations (Fig. 6a). The largest temperature increase over the Southern Ocean in austral winter (above 8 K) is a result of an increase in latent heat release in the atmosphere due to a reduction of sea-ice cover and an intensification of meridional moisture transport in the atmosphere. Warming in boreal latitudes in the Northern Hemisphere and in the tropics has a much less pronounced seasonal cycle. Seasonal changes in precipitation in the tropics follow absolute precipitation. The model simulates a strong amplification of summer monsoons (Fig. 6b). This is due to a stronger warming over land than over oceans, which increases moisture convergence over the continents in the tropics. In the high latitudes of the Southern Hemisphere the maximum increase of precipitation takes place in austral winter, while in the Northern Hemisphere the seasonal cycle is less pronounced. In the southern subtropics precipitation decreases during a large part of the year. The model predicts a decrease of cloudiness in the low latitudes, while in the high latitudes cloudiness increases in winter and decreases in summer (Fig. 6c). The model predicts the largest changes in soil humidity (Fig. 6d) in boreal latitudes of the Northern Hemisphere. Due to an increase of winter precipitation, and as a result, increase of snow thickness, there is an increase of soil moisture in spring just after the melting of snow. In summer, the increase of precipitation is not sufficient to compensate the increase of evaporation due to warming and soil moisture decreases. This is a rather robust result for the majority of GCMs. The model reveals strong changes in the cryosphere for a doubling of CO_2. In particular the annually average area of sea ice decreases by 31% (both in the Northern and Southern Hemisphere). The annual area covered by snow decreases by about 22%. Both these factors contribute to the decrease of surface and planetary albedo (see Table 2).

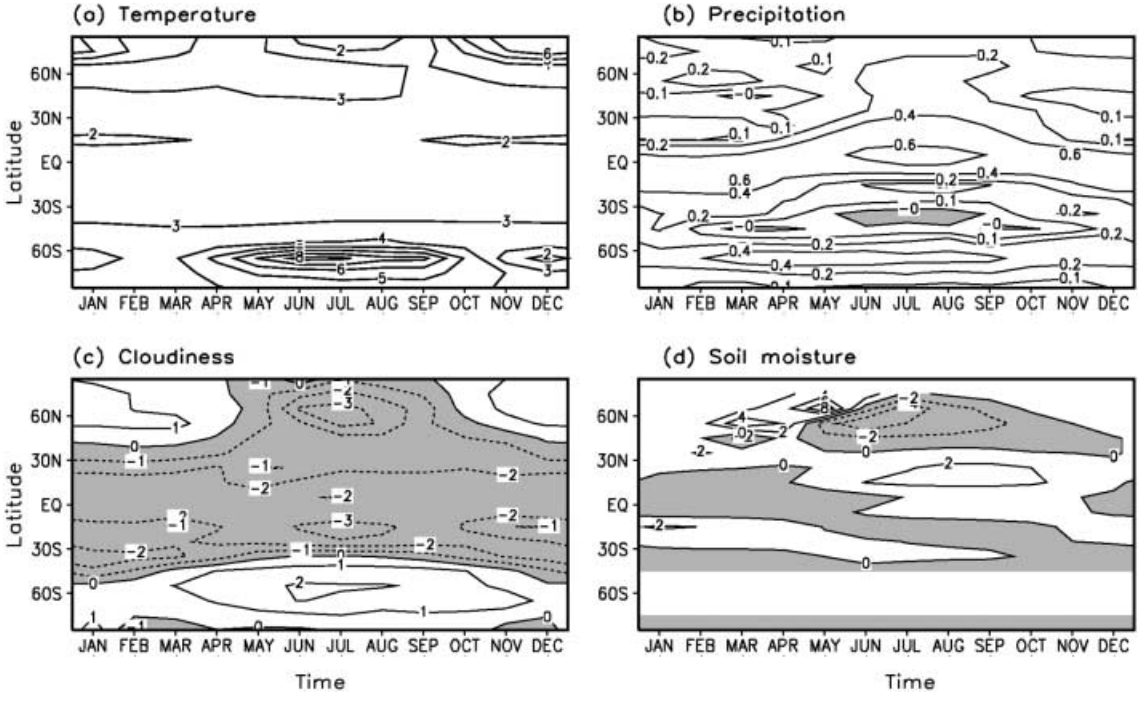

Fig. 6 Zonally averaged seasonal changes of **a** air temperature in K, **b** precipitation mm/day, **c** cloudiness in % and **d** soil moisture in cm for the equilibrium $2 \times CO_2$ experiment

3.2 Transient response

In Rahmstorf and Ganopolski (1999) we described the long-term future climate change simulations using CO_2 scenarios based on the historical trends and one of the IPCC 1992 projections. Here, for the purpose of comparing our results with most of the GCM experiments, we performed two experiments with 1% per year increase of CO_2 concentration. In the first, CO_2 was stabilised after 70 years of integration, when it reaches a level of twice the preindustrial concentration of 280 ppm used in the control simulation. In the second, CO_2 was stabilised after 140 years at a level of four times the preindustrial. The total duration of each experiment was 4000 years, thus the climate state obtained at the end of the integrations is very close to equilibrium.

Figure 7 shows the transient response of global air temperature, sea level and intensity of Atlantic thermohaline circulation to the changes in CO_2 concentration. The results of the transient runs are very similar to those obtained with coupled GCMs. After a decadal delay (''cold start problem'', Hasselmann et al. 1993) the temperature starts to rise almost linearly at a rate of about 0.3 K per decade and reaches 63% of its equilibrium warming at the time of CO_2 doubling, which is within the range of the coupled GCM results (50–80%, Houghton et al. 1996). Sea level rises due to thermal expansion by about 30 cm in the first hundred years of a 1% increase of CO_2 (a number close to IPCC 1995 best fit). Equilibrium increases of sea level are 154 cm and 285 cm for doubling and quadrupling of CO_2 concentration respectively. While after 500 years of integration the global air temperature approaches the equilibrium changes to within 5–10%, sea level rise is only one-half of its equilibrium response. Changes in thermohaline circulation will be discussed latter.

Figure 8 shows the temporal evolution of zonally averaged anomalies during a 1% increase of CO_2. Surface air temperature increases faster in the Northern Hemisphere than in the Southern Hemisphere. This is a

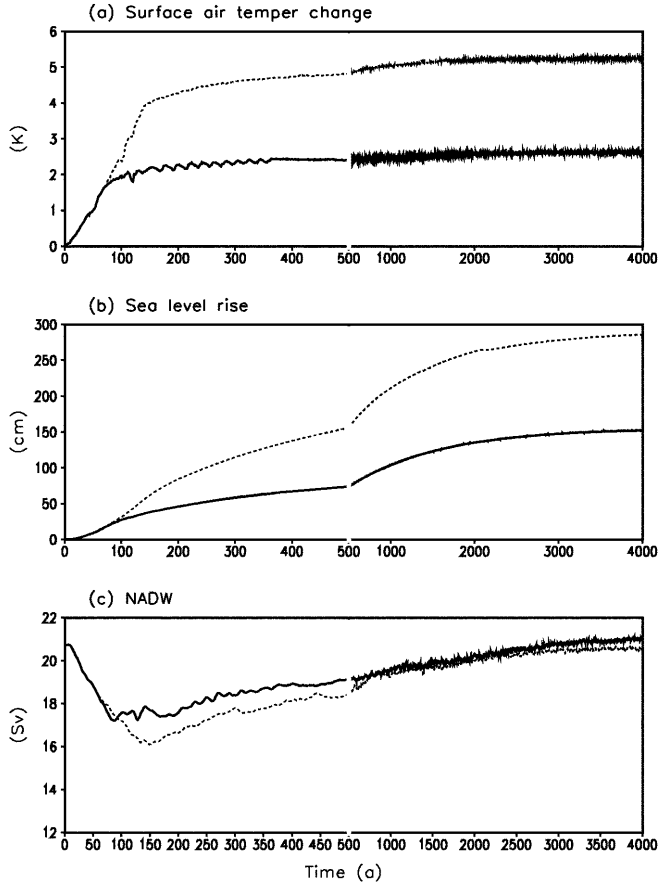

Fig. 7a–c Transient response to a 1% increase to the levels $2 \times CO_2$ (CT2, *solid line*) and $4 \times CO_2$ (CT4, *dashed line*) for globally and annually averaged anomalies of **a** surface air temperature, **b** sea level rise, and **c** maximum of the North Atlantic overturning in Sv. Note the changes in *time axis scale* after year 500

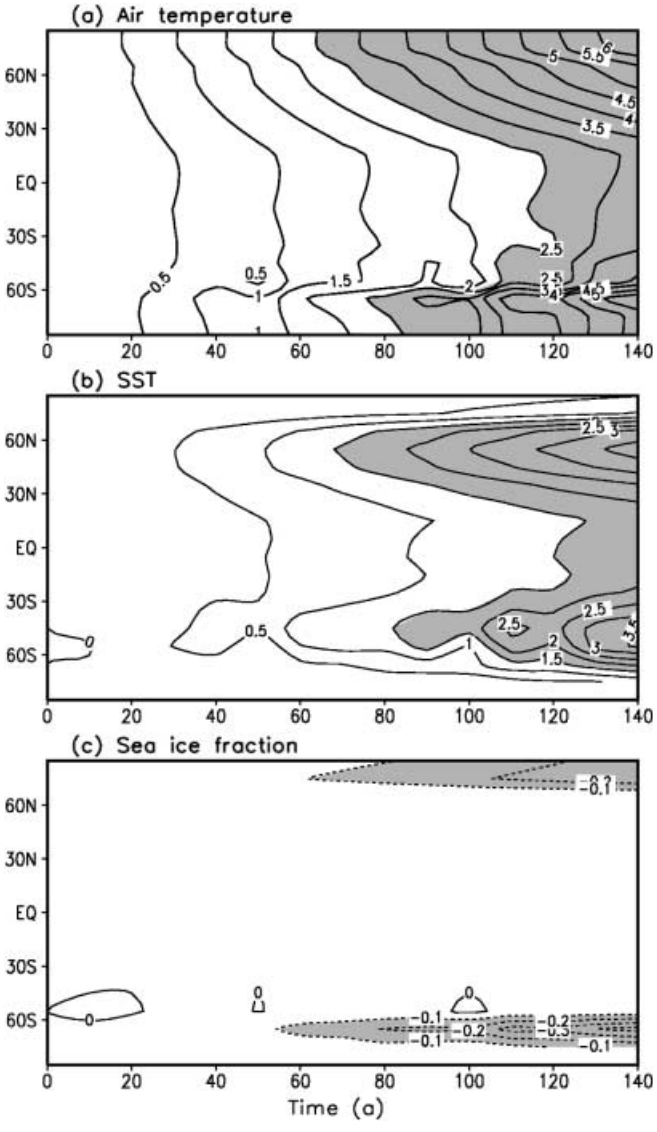

Fig. 8a–c Transient response to 1% increase of CO_2 concentration (experiment CT4) of zonally averaged **a** annual surface temperature, **b** SST and **c** sea-ice fraction

well-known interhemispheric asymmetry (Bryan et al. 1988) caused by the difference in ocean cover of the two hemispheres. Although all models show this phenomenon, they differ in degree of this asymmetry. In the GFDL model (Manabe et al. 1991) Northern Hemisphere temperature increases almost twice as fast as in the Southern Hemisphere. In our simulations the rates of temperature change in the two hemispheres differ to a lesser degree (30%). One of the reasons for the very slow southern warming in coupled GCM simulations is deep convection in the Southern Ocean, which increases the thermal inertia of the Southern Hemisphere (SH). Using the Gent and McWillams parameterisation instead of horizontal diffusion in some AOGCMs led to a reduction of convection in the Southern ocean and, as a result, to an increase in the rate of warming in the SH (Mitchell et al. 1998). In our model, although we use horizontal diffusion, convection is rather shallow in the Southern Ocean which allows SST in both hemispheres to rise at comparable rate (Fig. 8b).

3.3 Changes in thermohaline circulation

Figure 7c shows the temporal evolution of the strength of the thermohaline circulation (maximum of overturning in the Northern Hemisphere). Overturning gradually weakens with the increase of CO_2 and reaches its minimum soon after CO_2 is stabilised in both cases. For a doubling of CO_2 our model shows a 15% decrease of thermohaline circulation, and for a quadrupling a 25% decrease. In both cases, after stabilisation of the CO_2 concentration the thermohaline circulation gradually recovers and after a few thousand years returns to its initial intensity.

Manabe and Stouffer (1994) reported a much stronger impact of global warming on the thermohaline circulation. In their experiment, for a quadrupling of the CO_2 concentration the thermohaline circulation collapsed within a few hundred years and stayed in a conveyor-off mode for centuries at least. Similar experiments performed later with other coupled GCMs (see Rahmstorf 1999) show a decline of the thermohaline circulation in response to global warming, but only a few of these experiments are long enough to draw conclusions about the ultimate state of the thermohaline circulation. In a few sufficiently long simulations (e.g. Wood et al. 1999) thermohaline circulation survives a quadrupling of CO_2 concentration. There is also an ambiguity in the possible mechanisms of a weakening of the thermohaline circulation. Dixon et al. (1999) demonstrated that the weakening of thermohaline circulation in the GFDL coupled model can be attributed primarily to changes in freshwater flux, while temperature changes play only a secondary role. In contrast, Mikolajewicz and Voss (2000) reported temperature changes as the primary mechanism for the reduction of the thermohaline circulation in the ECHAM3/LSG coupled model.

In Rahmstorf and Ganopolski (1999) we speculated that the differences in the response of the thermohaline circulation to global warming could be, at least partly, attributed to the large differences in the changes in hydrological cycle. We proposed a new diagnostic quantity, that we termed "Atlantic hydrological sensitivity", which could be helpful in quantifying these differences. We defined it as the change in the freshwater flux to the North Atlantic (northward of 50°N) per degree of annual warming in the Northern Hemisphere. Figure 9 shows that the changes in the simulated freshwater flux into the North Atlantic and warming of the Northern Hemisphere are well correlated in our model. Roughly half of the increase of the freshwater flux is attributed to the increase in run-off, which is consistent with the results of the GFDL model (Dixon et al. 1999). However, the absolute changes in the freshwater flux in the GFDL model are much stronger than in CLIMBER-2. While the hydrological sensitivity of our model is 0.013 Sv/K, the GFDL model has hydrological sensitivity of 0.030 Sv/K. The latest version of the Hadley Centre model, HadCM-3 (Wood et al. 1999), has a hydrological sensitivity in between the former two (0.020 Sv/K, where no contribution from melting of Greenland Ice is included). It is too early to say now whether these numbers cover the whole range of uncertainties in the hydrological sensitivity.

The difference in hydrological sensitivities between our model and the GFDL model allows us to understand the differences in the contribution of the different factors (temperature and salinity changes) to the weakening of the thermohaline circulation. Figure 10 shows changes in Atlantic temperature, salinity, density and overturning at the time of quadrupling of CO_2. The largest changes in the thermohaline circulation are in the Northern Hemisphere, where overturning becomes weaker and its maximum is shifted towards the surface. This pattern is very similar to that simulated by coupled GCMs. It is clearly seen from Fig. 10 that temperature changes give the main contribution to the density

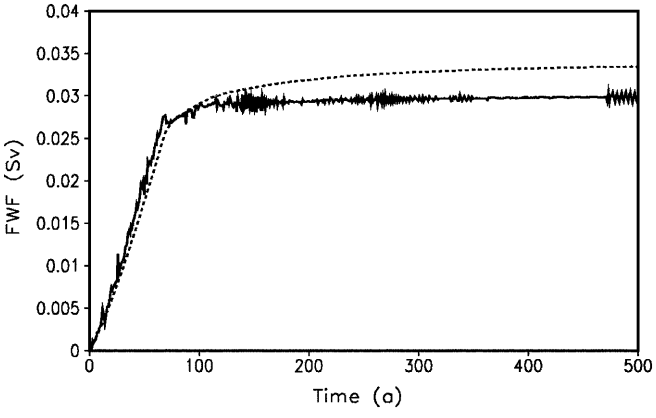

Fig. 9 Transient response of freshwater flux to the Northern Atlantic (*dashed line*) and changes in the Northern Hemisphere air temperature multiplied by the hydrological sensitivity of the model ($k = 0.013$ Sv/K) in experiment CT4

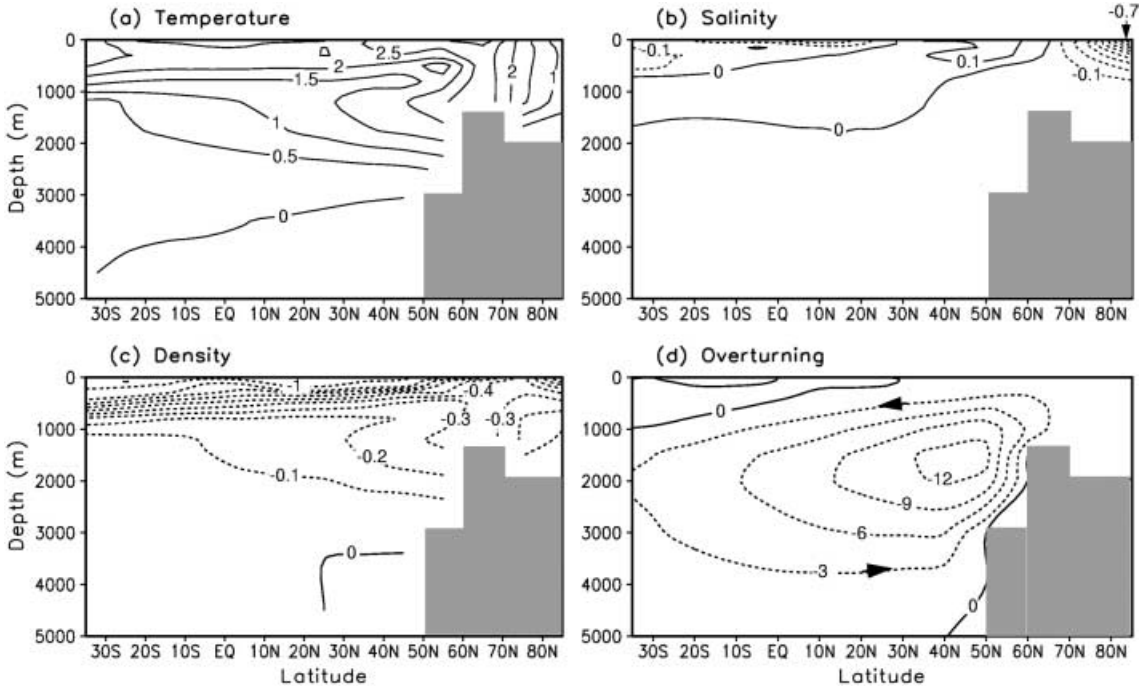

Fig. 10 Changes in zonally averaged **a** temperature, **b** salinity in ppt, **c** density in kg/m^3 and **d** meridional overturning stream function in Sv in the Atlantic in experiment CT4 at the time of quadrupling CO_2

changes. Similar to GCM experiments (Manabe and Stouffer 1994; Cai and Gordon 1998), salinity decreases in the high northern latitudes and increases in the subtropics, but in our case these changes contribute only 10% to the changes in the meridional density gradients.

If we increase the effective hydrological sensitivity in the same way as in Rahmstorf and Ganopolski (1999) to the level of the GFDL model (i.e. roughly by a factor of three, an experiment referred hereafter as EHS) the thermohaline circulation responds strongly to an increase of CO_2 concentration (Fig. 11). While during the first few decades there is no substantial difference between CT4 and CT4_EHS experiments, the maximum reduction of the thermohaline circulation is twice as large in CT4_EHS as in CT4. In the CT4_EHS experiment the role of the thermal component decreases, while the role of salinity increases in comparison to CT4, and at the time of quadrupling of CO_2, the changes in salinity are responsible for almost half of the decrease in the thermohaline circulation. However, even with enhanced hydrological sensitivity the thermohaline circulation does not collapse and gradually recovers after stabilisation of CO_2. A possible explanation for the stable conveyor in this experiment is that the initial thermohaline circulation is too strong and oceanic heat transport is large enough to sustain deep convection in the northern North Atlantic even with enhanced hydrological sensitivity. To test this hypothesis, we decreased vertical diffusivity in our model to the level of the GFDL model (from 0.5 to 0.3 cm^2/s in upper ocean and from 1.5 to 1.3 in the deep ocean) and repeated the experiments with original and enhanced hydrological sensitivity for the same quadrupling of CO_2 scenario (experiments referred as CT4_SVD and CT4_SVD_EHS hereafter). The reduction of vertical diffusion decreases the maximum of overturning in the Atlantic to 17 Sv for present-day CO_2 level. Other characteristics of climate are little changed. In the CT4_SVD experiment, the thermohaline circulation decreases at a similar rate to the CT4 experiment (Fig. 11). This indicates that the rate of 3–5 Sv per century of the decline of the thermohaline circulation due to the thermal effect is rather robust. The combination of lower

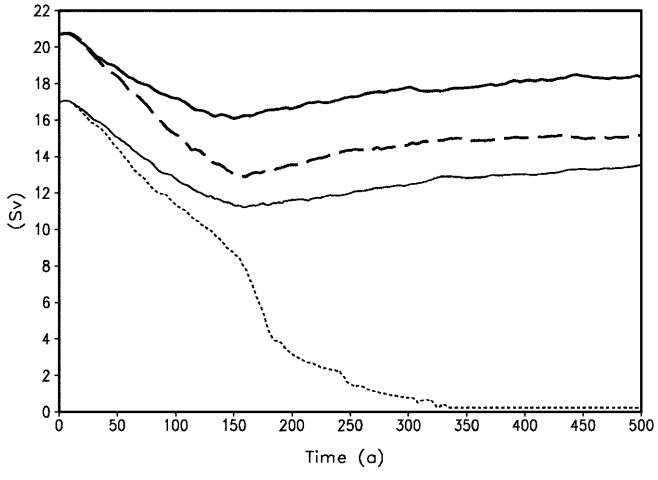

Fig. 11 Transient response of the meridional overturning stream function in Sv in the Atlantic to a 1% increase of CO_2 concentration to the level $4 \times CO_2$ in experiments CT4 (*thick solid line*), CT4_EHS (*thick dashed line*), CT4_SVD (*thin solid line*), and CT4_EHS_SVD (*thin dashed line*)

vertical diffusion and higher hydrological sensitivity (experiment CT4_SVD_EHS) leads to an irreversible collapse of the thermohaline circulation. The temporal evolution of the thermohaline circulation in this experiment is very similar to Manabe and Stouffer (1994). These results show that the long-term evolution of the thermohaline circulation depends on a combination of factors: CO_2 scenario, hydrological sensitivity of the atmosphere model, and threshold of convective instability in the ocean model.

4 Sensitivity to the solar variability

Variability of the solar constant on time scales from decades to centuries within a range of a few W/m^2 produces direct radiative forcing, which contributes to natural climate variability and can mask the anthropogenic climate change. Recently a study of the response of the climate system to changes in solar constant during the last three centuries was performed using the coupled climate GCM ECHAM-3/LSG (Cubasch et al. 1997). It allows us to make direct comparison of CLIMBER-2 transient response with the results of a more comprehensive model using identical forcing (Hoyt and Schaten 1993). Figure 12a shows the variability of solar constant from 1700 to 1992 used as forcing for the model. Since the initial value of the solar constant (at the year 1700) is different from that used in the control run of CLIMBER-2 (1365 W/m^2, the same as in ECHAM-3), we use the same procedure as in Cubasch et al. (1997), namely a 20-year linear adjustment from control solar insolation to that corresponding to the year 1700. Figure 12b shows a comparison of the temporal variation of the globally averaged annual surface air temperature anomalies simulated by CLIMBER-2 and ECHAM3/LSG. Both curves represent the average of two runs performed with the same forcing but slightly different initial conditions. Agreement between the results of the two models is fairly good, considering that CLIMBER-2 by design has a much smaller internal climate variability. In particular, both models show a warming by about 0.2 K during the twentieth century due to the increase of solar insolation. Cubasch et al. (1997) reported a larger response of ECHAM3/LSG to a decrease in solar radiation compared to an increase, while our model shows a symmetric response. This explains the differences between two models in the amplitude of the temperature minima around years 1700 and 1800. Global sensitivity to the variations in solar constant for both models is close to 0.07 K/(W m^{-2}), which is only half of the equilibrium response of CLIMBER-2 to a permanent change in solar constant (0.13 K/W m^{-2}). This is consistent with the fact that the sensitivity of CLIMBER-2 to doubling of CO_2 is almost identical to ECHAM3/LSG in respect of global air temperature changes. CLIMBER-2 has a smaller interannual variability compared to the GCM and shows a higher correlation (0.85 versus 0.67 in case of ECHAM3/LSG) between temperature and solar insolation. Similar to ECHAM3/LSG our model shows an anticorrelation between the changes in solar insolation and the intensity of the thermohaline circulation in the Northern Atlantic. The amplitude of the changes of thermohaline circulation in our model is about 5%, which half of that reported in Cubasch et al. (1997). The spatial distribution of the linear regression coefficients between annual air temperature changes and changes in solar constant, shown in Fig. 13, resembles the corresponding figure in Cubasch et al. (1997). The highest values of temperature response occur over the continents in the Northern Hemisphere and in the Arctic, where the sensitivity to the changes in solar constant is twice as large as for most of the oceans.

The tropics are characterised by a rather uniform sensitivity of around 0.05 K/(W m^{-2}). The weakest

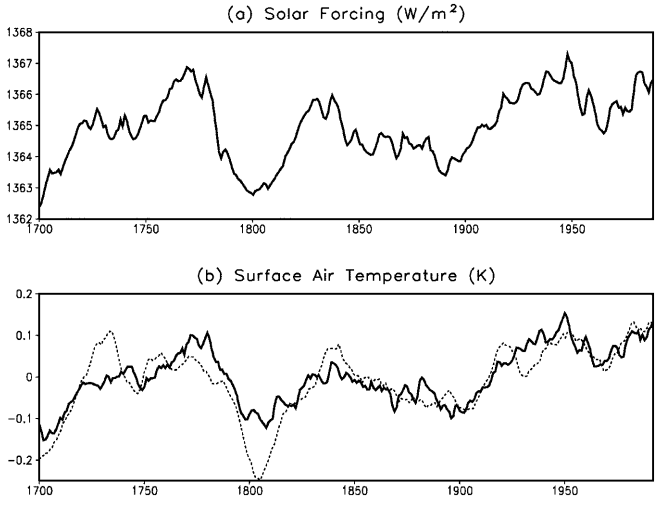

Fig. 12 Temporal variations (year 1700–1990) of **a** solar constant and **b** global annual air temperature. *Solid curve* shows CLIMBER-2 simulations, *dashed*-averaged of two ECHAM/LSG simulations (Cubasch et al. 1997)

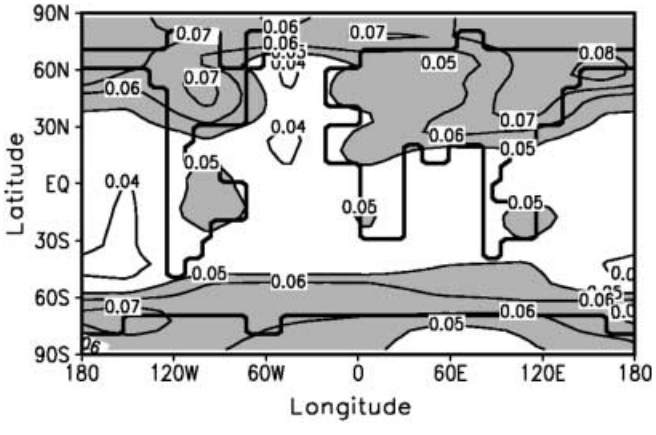

Fig. 13 Transient temperature response to changes in solar constant in K/(W m^{-2})

temperature response to the changes in solar constant is observed in the Southern Hemisphere, where it is attenuated by the large thermal inertia of the ocean. Unlike ECHAM3/LSG, our model does not have regions of negative correlation between temperature and forcing. Spatial patterns of temperature changes caused by an increase of the solar constant during the twentieth century are almost identical to those caused by the impact of CO_2 rise (correlation between annual temperature changes is 0.96), but CO_2 produces relatively stronger winter warming than solar variability. The vertical structure of atmosphere temperature changes due to changes in solar constant in the troposphere is very similar to that of CO_2 response, but in the stratosphere there is no cooling in the former case. This also agrees well with Cubasch et al. (1997).

5 Sensitivity to the changes in vegetation cover

Many recent studies show that changes in vegetation cover could substantially affect climate. Moreover feedback between climate changes (caused by external factors, like changes in orbital parameters) and changes in vegetation cover can amplify and modify the climate response (e.g. Harvey 1988; Berger et al. 1992) or even lead to multiple equilibria of the climate system (Claussen 1998). In particular, climate-vegetation feedbacks appear to be important for the explanation of the warmer and wetter climate during the mid-Holocene (TEMPO members 1996; Ganopolski et al. 1998b) and glacial inception around 115 000 years before present (e.g. Otterman et al. 1984; de Noblet et al. 1996). Anthropogenic deforestation may have contributed to the observed climatic changes. Here we consider two extreme scenarios, complete deforestation in the boreal zone and in the tropics. These scenarios are not intended to mimic any real changes in the past or future, but rather to represent a sensitivity test of the maximum influence of changes in vegetation cover on climate. Since similar experiments were performed with different GCMs, they give an opportunity to compare the sensitivity of our model with those of comprehensive climate models in this respect. For both scenarios we performed experiments with fixed and interactive ocean to show the importance of the ocean for the climate response to changes in vegetation cover.

5.1 Boreal deforestation experiment

Bonnan et al. (1992, 1995), compared the climate response to complete deforestation in the boreal zone in experiments with fixed SST and sea ice, and with a simple mixed-layer ocean model. Both experiments show cooling over the deforested area, but in the experiment with interactive ocean cooling was much stronger, more uniformly distributed over the year and much more geographically extended. In most of similar sensitivity experiments performed later (Polcher and Kaval 1994; Douville and Royer 1996) oceanic characteristics (SST and sea ice) were fixed.

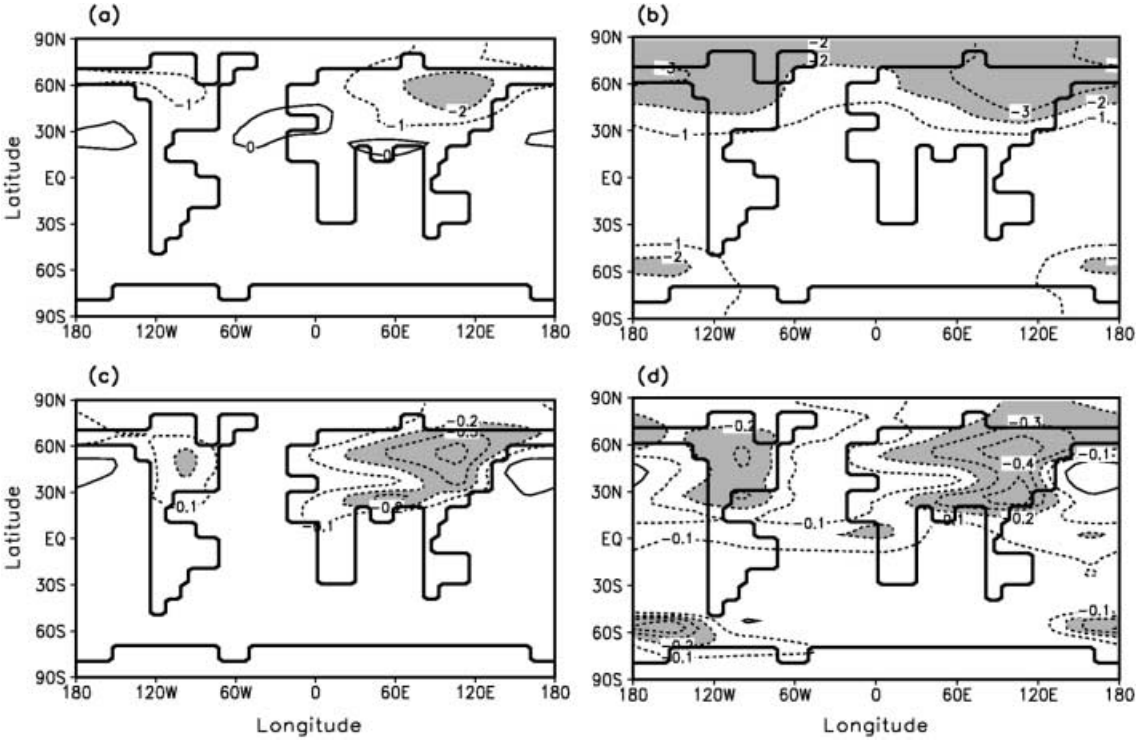

Fig. 14 Differences in **a, b** annual near surface air temperature in K and **c, d** precipitation in mm/day between boreal deforestation and control (CE) experiments. **a, c** Correspond to experiments with fixed ocean characteristics (BD_A), **b, d** to experiment with interactive ocean (BD_AO)

We performed two experiments similar to Bonan et al. (1995). In the first, all vegetation northward of 40°N was replaced by bare soil (boreal desertification experiment, referred as BD hereafter). In the second, all forest in this area was replaced by grass (experiment BG). For each of these land-cover changes we performed experiments with fixed ocean characteristics (atmosphere only, called BD_A and BG_A correspondingly) and with the fully coupled atmosphere-ocean model (referred to as BD_AO and BG_AO correspondingly). Results of the BD and BG experiments for the same configuration of the model (atmosphere only or coupled model) are very similar which agrees with Bonan et al. (1995). The reason is that the major impact of deforestation on climate in the boreal zone is due to the difference in winter albedo between forest and non-forest surface cover. Bare soil and grass differ little in respect of winter albedo in our model. At the same time, the results of experiments with fixed ocean and interactive ocean are rather different (see Fig. 14). Although in both experiments maximum annual cooling occurs in northeastern Asia, in the BD_AO experiment cooling is more pronounced and extended. Globally averaged temperature in the BD_AO experiment is 1 K lower than in the control, while in BD_A cooling is restricted to the area of deforestation and global cooling is only 0.2 K. In both the BD_A and BD_AO experiments (Fig. 15) maximum cooling occurs during spring and early summer, when the increase in surface albedo produces maximum radiative forcing (Fig. 16). The duration of the snow season increases by 1–2 months compared to the control experiment. In the BD_AO experiment cooling is more uniformly distributed over the year than

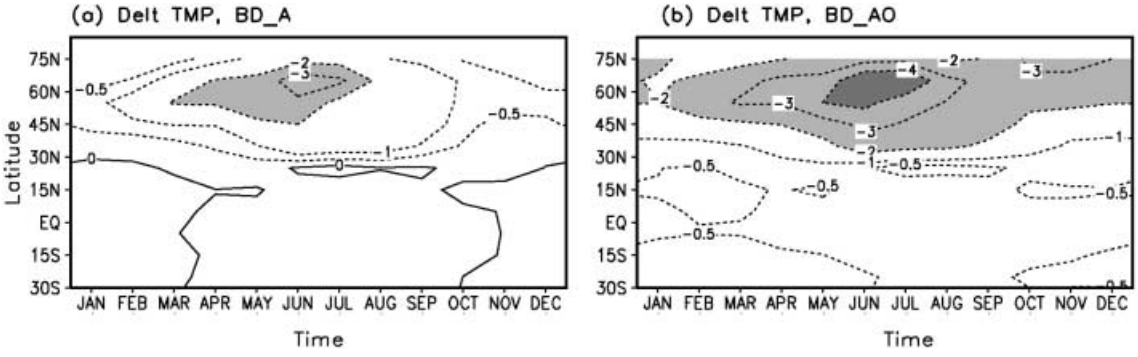

Fig. 15a, b Seasonal differences in the zonally averaged near surface surface air temperature over the continents between the boreal deforestation and control (CE) experiments for **a** BD_A, **b** and BD_AO

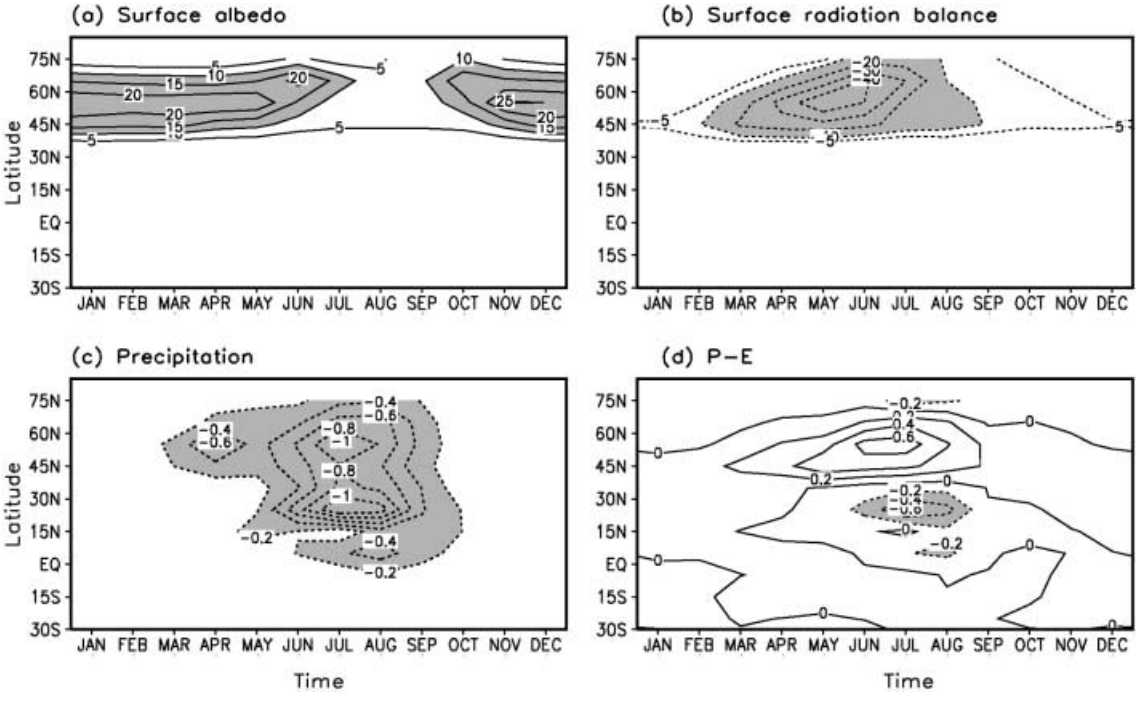

Fig. 16a–d Seasonal differences between the BD_AO and control (CE) experiments in the zonally averaged **a** surface albedo, **b** surface radiation balance in W/m^2, **c** precipitation in mm/day, and **d** *P-E* in mm/day, over the continents

in BD_A. This difference is primarily due to an increase in sea ice in the BD_AO experiment (annually by 20%) which produces a cooling effect over the whole year. These features of the A and AO experiments are qualitatively very similar to Bonan et al. (1992), but the temperature changes simulated in the latter are much stronger. On the other hand, the results of our BD_A experiments are very close to similar experiments by Chalita and Le Treut (1994) and Douville and Royer (1997). Due to the cooling in high latitudes of the Northern Hemisphere the intensity of the thermohaline circulation in the Atlantic is increased by 2 Sv and, as a result, northward heat transport increases in the Atlantic ocean. This negative feedback between thermohaline circulation and temperature explains why cooling over the North Atlantic and Europe is weaker than that over the Pacific and America for the same latitudes.

The hydrological cycle is also strongly affected by changes in vegetation cover. Precipitation decreases over the continents in boreal latitudes by 10%. Due to the reduction of transpiration, total evapotranspiration decreases even more strongly than precipitation and summer run-off increases. This reduction of local recirculation of precipitated water additionally contributes to the reduction of precipitation. Another area of substantial reduction of precipitation is southern and southeastern Asia (Fig. 14). The reason for the decrease of precipitation there is a weakening of the summer monsoon. Although this area is not directly affected by changes in vegetation cover, the cooling over Eurasia reduces the temperature gradient between continent and ocean, and as a result, decreases moisture convergency in this region (seen as a negative *P-E* anomaly in this region in Fig. 16d). A similar impact of the cooling over Asia on monsoon circulation was obtained in Douville and Royer (1996) and some other studies on the relation between winter snow cover anomalies in Asia and monsoon precipitation. Crowley and Baum (1997) further find a weakening of the Asian monsoon after a reduction of the forested area in Asia forthe Last Glacial Maximum.

5.2 Tropical deforestation

Studies of the impact of tropical deforestation on regional climate were performed with different atmospheric GCMs (e.g. Polcher and Kaval 1994; Sud et al. 1996; Lean and Rowntree 1997; Hahmann and Dickinson 1997). An atmosphere GCM coupled to a simple ocean mixed layer model was used for this type of study by Henderson-Sellers et al. (1993). Most of the models predict a strong decrease of precipitation over the deforested continents and an increase of surface air temperature, although they disagree in the amplitudes of this changes. Obviously the results are sensitive to the climatic properties of the surface cover type which was used as a substitution for tropical forest. To cover the whole range of these differences, we performed two series of experiments similar to those made for boreal deforestation. We performed (1) experiments with all vegetation in the tropics (between 20°S and 20°N) replaced by bare soil (experiments referred as TD), and (2) experiments with tropical forest replaced by grass (referred as TG). We also performed simulations with the atmosphere-only model with fixed ocean characteristics (TD_A, TG_A) and with the coupled atmosphere-ocean model (TD_AO, TG_AO). As in the previous case (boreal deforestation) there is a large difference between experiments with fixed and interactive ocean, but unlike the previous case the results of the TD and TG experiments also differ substantially. The changes in climate characteristics averaged over land in the latitudinal belt 10°S–10°N are presented in Table 3. Figure 17 shows the zonally averaged annual differences between two tropical desertification experiments (TD_A, TD_AO) and control run. Corresponding figures for the TG_A and TD_AO experiments (not shown) are similar but with smaller amplitudes, as is also seen from Table 3. In all experiments evaporation decreases over land due to the reduction of transpiration when the forest is gone. This leads to a reduction in cloudiness and precipitation. Absolute changes in precipitation and evaporation in all experiments are very close, thus moisture convergence over continents does not change. Reduction of cloudiness leads to an increase of incomimg solar radiation, but the absorbed solar radiation does not change much due to the increase of surface albedo. Downward longwave radiation strongly decreases due to the reduction of water vapour in the atmosphere and, as a result, the surface radiation balance decreases. Since latent heat flux from the surface decreases even more strongly than radiative balance, the difference is compensated for by an increase in sensible heat flux. All these changes are in agreement with most GCM experiments.

Table 3 Annual mean changes in climate characteristics due to tropical deforestation in the latitudinal belt between 10°S and 10°N. All characteristics except for SST are averaged only over the land. Numbers in brackets show relative (to the absolute values at present-day) changes

	TD_A	TD_AO	TG_A	TG_AO
Δ T_a, K	+1.2	+0.5	+0.4	+0.1
Δ precipitation, mm/d	−2.5 (−38%)	−2.6 (−41%)	−1.0 (−15%)	−1.1 (−17%)
Δ evaporation, mm/d	−2.7 (−60%)	−2.8 (−61%)	−1.1 (−23%)	−1.1 (−25%)
Δ cloudiness, %	−14	−14	−5	−5
Δ surface absorbed SW radiation, W/m^2	1	2	−1	−1
Δ surface radiation balance, W/m^2	−29	−28	−12	−12
Δ sensible heat flux, W/m^2	+50	+53	+19	+21
Δ SST, K	–	−0.6	–	−0.3

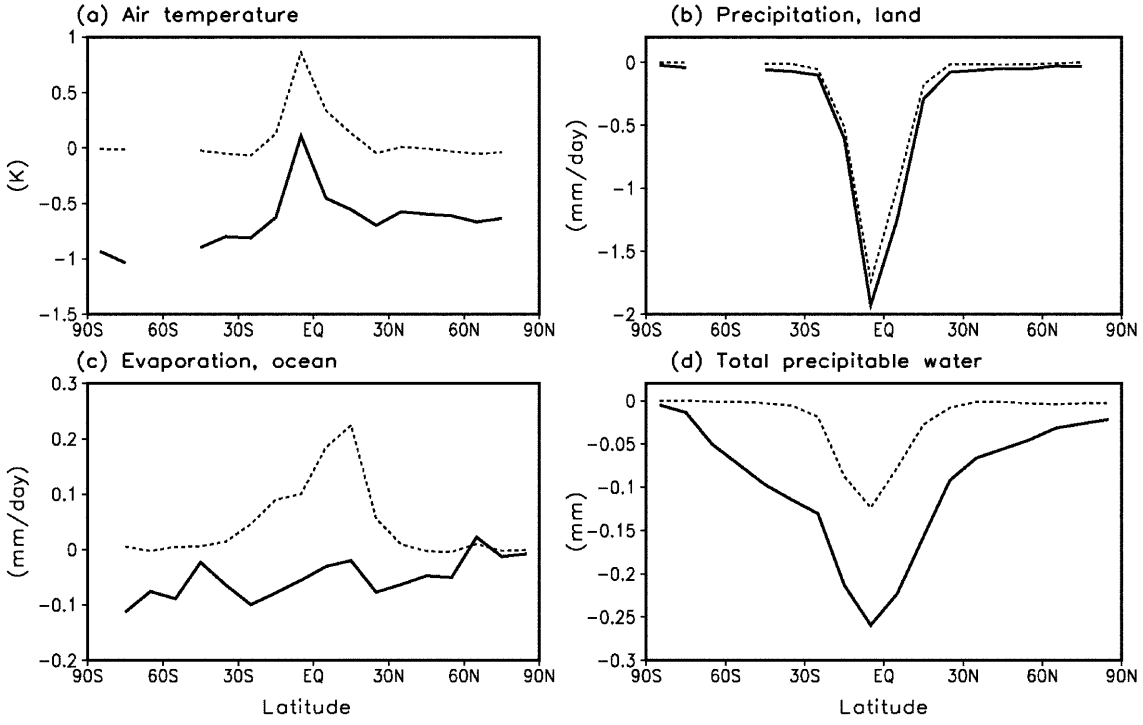

Fig. 17a–d Zonally averaged differences between tropical deforestation and control experiments for TD_AO (*solid line*) and TD_A (*dashed line*). **a** Differences in surface air temperature over land. **b** Changes in precipitation over land in mm/day. **c** Changes in evaporation over oceans in mm/day. **d** Changes in total precipitable water in the atmosphere in mm averaged over oceans and land

In the experiment with fixed SST, temperature over land increases in the tropics (Fig. 17). Obviously, there are few changes over the ocean in these experiments. In the experiment with an interactive ocean the picture is rather different. Positive temperature anomalies in the tropics practically disappear and global air temperature drops by 0.5 K in TD_AO, and 0.2 K in TG_AO. The reason for the global cooling due to tropical deforestation is a strong reduction of downward longwave radiation, caused by the reduction of water vapour content in the atmosphere. Figure 17d shows that in the TD_A experiment this reduction (as well as other changes) is located in the tropics. In the TD_AO experiment reduction of precipitable water in the atmosphere is much stronger in the tropics and extends far beyond the tropics. Figure 17c shows the differences in the reaction of evaporation from the ocean in these two experiments. In the experiment with fixed ocean, evaporation from the ocean in the tropics increases and approximately compensates for a decrease of evaporation from the land. The interactive ocean reacts to the decrease of water content in the atmosphere by a cooling and a decrease in evaporation that amplifies the decrease in the water vapour greenhouse effect. This results indicates that the interactive ocean can substantially modify the response to tropical deforestation. Although a similar set of experiments has not been performed with GCMs, the very small temperature response in the tropics simulated in experiments with mixed layer ocean (Henderson-Sellers et al. 1993), compared to other experiments with fixed ocean, seems to support our finding.

6 Conclusions

1. We have presented the results of a series of sensitivity experiments performed with the climate system model of intermediate complexity, CLIMBER-2. The results were compared with corresponding experiments performed with atmosphere, ocean and coupled GCMs. The dual purpose of our work was (a) to demonstrate that the model is able to mimic the dynamical properties of much more sophisticated and computationally expensive models, and (b) to illustrate the potential of the climate model of intermediate complexity to contribute to a better understanding of climate dynamics.

2. The study of the sensitivity of the Atlantic thermohaline circulation to changes in freshwater flux shows that CLIMBER-2 has similar stability properties to a GCM. For the standard set of parameters the model has two equilibria corresponding to the conveyor-on and -off modes of thermohaline circulation. Differences between these two states in respect of temperature, precipitation and atmospheric dynamics are similar to those simulated with coupled GCMs. We have shown that an increase of vertical diffusivity in the ocean changes the stability properties of the model. In this case it has only one equilibrium, in agreement with the results of the GFDL model. Our results sug-

gest that a positive feedback between thermohaline circulation and freshwater flux does not play an important role.

3. The model shows equilibrium and transient responses to the changes in CO_2 concentration similar to other models, with respect to temperature, hydrological cycle, changes in cryosphere and ocean characteristics. Due to shallow convection in the Southern Ocean the model reveals relatively weak interhemispheric asymmetry compared to some GCMs. We have shown that the reduction of North Atlantic overturning in our model is primarily due to a thermal effect, while changes in salinity play a minor role. We argue that this difference with the GFDL model is due to much smaller hydrological sensitivity in our model, and we have shown that when the hydrological sensitivity is increased and vertical diffusivity decreased to the values of the GFDL model, results of the two models become very similar.

4. In the experiment with temporal variability of the solar constant the model simulates anomalies in the globally averaged temperature in good agreement with the ECHAM3/LSG coupled model, except for two cooling events. CLIMBER-2 results indicate that about 0.2 K warming during the twentieth century can be explained by solar variability, which is consistent with the GCM results. The results of both models are, at least qualitatively, similar with respect to the spatial patterns of the temperature response to solar variability, as well as in the changes in the ocean thermohaline circulation.

5. The series of simulations of climate sensitivity to deforestation in the boreal zone and in the tropics indicate the important role of vegetation in the climate system. The results of these simulations are in agreement with the results of GCM experiments performed in a similar configuration. Our results illustrate the important role of the ocean in amplification or modification of the climatic response to changes in vegetation cover via water vapour and ice-albedo feedbacks. It has been shown that in the coupled climate model both boreal and tropical deforestation lead to global cooling, while an atmosphere-only version of the model predicts different signs of temperature changes in these experiments. In our simulations boreal deforestation leads to a weakening of subtropical monsoons in the Northern hemisphere.

6. The overall conclusion from all these sensitivity experiments is that CLIMBER-2, in spite of its coarse spatial resolution and simplicity in the description of individual processes, is able to simulate the climate response to changes in different types of forcing and boundary conditions in reasonable agreement with the results of the state-of-the art GCMs. The work also illustrates how models of intermediate complexity can be used for a better understanding of the interaction between different components of the climate system, as well as for explaining of the discrepancies among the results obtained with different complex models.

References

Bertrand C, van Ypersele J-P, Berger A (1999) Volcanic and solar impacts on climate since 1700. Clim Dyn 15: 355–367

Bonan GB, Pollard D, Thompson SL (1992) Effect of boreal forest vegetation on global climate. Nature 359: 716–718

Bonan GB, Chapin FS, Thompson SL (1995) Boreal forest and tundra ecosystems as components of the climate system. Clim Change 29: 145–167

Berger A, Fichefet Te, Gallee H, Tricot Ce, van Ypersele J-P (1992) Entering the glaciation with a 2-D coupled climate model. Quat Sci Rev 11: 481–493

Brovkin V, Ganopolski A, Claussen M, Kubatzki C, Petoukhov V (1999) Modelling climate response to historical land cover change. Global Ecol Biogeogr 8: 509–517

Bryan F (1986) High-latitude salinity effects and interhemispheric thermohaline circulations. Nature 323: 301–304

Bryan K, Manabe S, Spelman MJ (1988) Interhemispheric asymetry in the transient response of a coupled ocean-atmospheric model to a CO_2 forcing. J Phys Oceanogr 18: 851–867

Cai W, Gordon HB (1998) Transient responses of the CSIRO climate moel to two different rates of CO_2 increase. Clim Dyn 14: 503–516

Claussen M (1998) On multiple solutions of the atmosphere-vegetation system in present-day climate. Global Change Biol 4: 549–559

Claussen M, Kubatzki C, Brovkin A, Ganopolski A, Hoelzmann P, Pachur H-J (1999) Simulation of an abrupt change in Sahara vegetation in the mid-Holocene. Geophys Res Lett 26: 2037–2040

Chalita S, Le Treut H (1994) The albedo of temperate and boreal forest and the northern hemisphere climate: a sensitivity experiment using the LMD GCM. Clim Dyn 10: 231–240

Crowley TJ, Baum SK (1997) Effect of vegetation on an ice-age climate model simulation. J Geophys Res 12(D14): 16 463–16 480

Cubasch U, Hasselman K, Hock H, Maier-Reimer U, Mikolajewiccz U, Santer BD, Sausen R (1992) Time-dependent greenhouse warming computation with a coupled ocean-atmosphere model. Clim Dyn 8: 55–69

Cubasch U, Voss R, Hegerl GC, Waszkewitz J, Crowley TJ (1997) Simulation of the influence of solar radiation variations on the global climate with an ocean-atmosphere general circulation model. Clim Dyn 13: 757–767

Dixon KW, Delworth TL, Spelman MJ, Stoufer RJ (1999) The influence of transient surface fluxes on North Atlantic overturning in a coupled GCM climate change experiment. Geophys Res Lett 26: 2749–2752

Douville H, Royer J-F (1996) Sensitivity of the Asian summer monsoon to an anomalous Eurasian snow cover within the Meteo-France climate model. Clim Dyn 12: 449–466

Douville H, Royer J-F (1997) Influence of the temperate and boreal forests on the Northern Hemisphere climate in the Meteo-France climate model. Clim Dyn 13: 57–74

Fanning AF, Weaver AJ (1997) Temporal-geographical meltwater influence on the North Atlantic conveyor: implication for the Younger Dryas. Paleoceanography 12: 307–320

Ganopolski A, Rahmstorf S, Petoukhov V, Claussen M (1998a) Simulation of modern and glacial climates with a coupled model of intermediate complexity. Nature 391: 351–356

Ganopolski A, Kubatzki C, Claussen M, Brovkin V, Petoukhov V (1998b) The influence of vegetation-atmosphere-ocean interaction on climate during mid-Holocene. Science 280: 1916–1919

Hahmann AN, Dickinson RE (1997) RCCM2 BATS model over tropical South America: applications to tropical deforestation. J Clim 10: 1944–1964

Harvey LD (1988) On the role of high latitude ice, snow and vegetation feedbacks in the climatic response to external forcing changes. Clim Change 13: 191–224

Hasselmann K, Sausen R, Maier-Reimer E, Voss R (1993) On the cold start problem in transient simulations with coupled ocean-atmosphere models. Clim Dyn 9: 53–61

Henderson-Sellers A, Dickinson RE, Durbridge T, Kennedy P, McGuffie K, Pitman A (1993) Tropical deforestation: modelling local and regional-scale climate change. J Geophys Res 98(D4): 7289–7315

Houghton JT, Jenkins GJ, Ephraums JJ (1990) Climate change: the IPCC scientific assessment. Cambridge University Press, Cambridge, UK

Houghton JT, Meira Filho LG, Callander BA, Harris N, Kattenberg A, Maskell K (1996) Climate change 1995- the science of climate change. Cambridge University Press, Cambridge, UK

Hoyt DV, Schaten KH (1993) A discussion of plausible solar irradiance variations, 1700–1992. J Geophys Res 98A: 18 895–18 906

Hughes TMC, Weaver AJ (1996) Sea surface temperature – evaporation feedback and the ocean's thermohaline circulation. J Phys Oceanogr 26: 644–654

Kittel TGF, Giorgi F, Meehl GA (1998) Intercomparison of regional biases and doubled CO_2-sensitivity of coupled atmosphere-ocean general circulation model experiments. Clim Dyn 14: 1–15

Lean J, Rowntree PR (1997) Understanding the sensitivity of a GCM simulation of Amazonian deforestation to the specification of vegetation and soil characteristics. J Clim 10(6): 1216–1235

Manabe S, Stouffer RJ (1988) Two stable equilibria of a coupled ocean-atmosphere model. J Clim 1: 841–866

Manabe S, Stouffer RJ (1994) Multiple-century response of a coupled ocean-atmosphere model to an increase of atmospheric carbon dioxide. J Clim 7: 5–23

Manabe S, Stouffer RJ (1999) Are two modes of thermohaline circulation stable? Tellus 51A: 400–411

Manabe S, Wetherald RT (1987) Large-scale changes of soil wetness induced by an increase in atmospheric carbon dioxide. J Atmos Sci 44: 1211–1235

Manabe S, Stouffer RJ, Spelman MJ, Bryan K (1991) Transient response of a coupled ocean-atmosphere model to gradual changes of atmospheric CO_2. Part I: annual mean response. J Clim 4: 785–818

Mikolajewicz U, Voss R (2000) The role of the individual air-sea flux components in CO_2-induced changes of the ocean's circulation and climate. Clim Dyn 16: 627–642

Mitchell JFB, Johns TC, Senior CA (1998) Transient response to increasing greenhouse gases using model with and without flux adjustment. Hadley Centre Technical Note, UK

Nakamura M, Stone PH, Marotzke J (1994) Destabilization of the thermohaline circulation by atmospheric eddy transports. J Clim 7: 1870–1882

de Noblet N, Prentice IC, Jousaume S, Texier D, Bota A, Haxeltine A (1996) Possible role of atmosphere-biosphere interactions in triggering the last glaciation. Geophys Res Lett 23: 3191–3194

Otterman J, Chou MD, Arking A (1984) Effects of nontropical forest cover on climate. J Clim Appl Meteorol 23: 762–767

Petoukhov V, Ganopolski A, Brovkin V, Claussen M, Eliseev A, Kubatzki C, Rahmstorf S (2000) CLIMBER-2: a climate system model of intermediate complexity. Part I: model description and performance for present climate. Clim Dyn 16: 1–17

Polcher J, Kaval K (1994) A statistical study of the regional impact of deforestation on climate in the LMD GCM. Clim Dyn 10: 205–219

Rahmstorf S (1996) On the freshwater forcing and transport of the Atlantic thermohaline circulation. Clim Dyn 12: 799–811

Rahmstorf S (1999) Shifting seas in greenhouse? Nature 399: 523–524

Rahmstorf S, Ganopolski A (1999) Long-term global warming simulations with efficient climate model. Clim Change 43: 353–367

Schiller A, Mikolajewicz U, Voss R (1997) The stability of the North Atlantic thermohaline circulation in a coupled ocean-atmosphere general circulation model. Clim Dyn 13: 325–347

Schlesinger ME, Mitchell JFB (1987) Climate model simulations of the equilibrium climatic response to increase carbon dioxide. Rev Geophys 25: 760–798

Scott JR, Marotzke J, Stone PH (1999) Interhemispheric thermohaline circulation in a coupled box model. J Phys Ocean 29: 351–365

Sokolov AP, Stone PH (1998) A flexible climate model for use in integrated assesment. Clim Dyn 14: 291–303

Stocker TF, Schmittner A (1997) Influence of CO_2 emission rates on the stability of the thermohaline circulation. Nature 388: 862–865

Stocker TF, Wright DG (1991) Rapid transitions of the ocean's deep circulation induced by changes in surface water fluxes. Nature 351: 729–732

Sud YC, Walker GK, Kim J-H, Liston GE, Sellers PJ, Lau WK-M (1996) Biogeophysical consequences of a tropical deforestation scenario: a GCM simulation study. J Clim 9: 3225–3247

TEMPO members (1996) Potential role of vegetation feedback in the climate sensitivity of high-latitude regions: a case study at 6000 years BP. Global Biogeochem Cycle 10: 727–736

Thompson SL, Pollard D (1995) A global climate model (GENESIS) with a land-surface transfer sheme (LSX). Part II: CO_2 sensitivity. J Clim 8: 1104–1121

Washington WM, Meehl GA (1984) Seasonal cycle experiment on the climate due to a doubling of CO_2 with an atmospheric general circulation model coupled to a simple mixed-layer ocean model. J Geophys Res 89: 9475–9503

Wood R, Keen A, Mitchel JFB, Gregory JM (1999) Changing spatial structure of the thermohaline circulation in response to atmospheric CO_2 forcing in a climate model. Nature 399: 572–575